Neuropathology and
Applied Neurobiology **WILEY**
JOURNAL OF THE BRITISH NEUROPATHOLOGICAL SOCIETY

Simultaneous *Nbs1* and *p53* inactivation in neural progenitors triggers high-grade gliomas

David E. Reuss[1,2,3] | Susanna M. Downing[4] | Cristel V. Camacho[4] |
Yong-Dong Wang[4] | Rosario M. Piro[5] | Christel Herold-Mende[6] |
Zhao-Qi Wang[7,8] | Thomas G. Hofmann[9] | Felix Sahm[1,2,3] [ID] |
Andreas von Deimling[1,2,3] | Peter J. McKinnon[4] | Pierre-Olivier Frappart[9]

[1]Clinical Cooperation Unit Neuropathology, German Cancer Research Center (DKFZ), Heidelberg, Germany

[2]Consortium for Translational Cancer Research (DKTK), Heidelberg, Germany

[3]Department of Neuropathology, Institute of Pathology, Ruprecht-Karls-Universität Heidelberg, Heidelberg, Germany

[4]Center for Pediatric Neurological Disease Research, St. Jude Translational Neuroscience, Departments of Genetics and Cell and Molecular Biology, St. Jude Children's Research Hospital, Memphis, Tennessee, USA

[5]Dipartimento di Elettronica, Informazione e Bioingegneria (DEIB), Politecnico di Milano, Milan, Italy

[6]Department of Neurosurgery, Ruprecht-Karls-Universität Heidelberg, Heidelberg, Germany

[7]Leibniz Institute on Ageing-Fritz Lipmann Institute, Jena, Germany

[8]State Key Laboratory of Microbial Technology, Shandong University, Qingdao, China

[9]Institute of Toxicology, University Medical Center of the Johannes Gutenberg University Mainz, Mainz, Germany

Correspondence
Pierre-Olivier Frappart, Institute of Toxicology, University Medical Center of the Johannes Gutenberg University Mainz, Mainz, Germany.
Email: pfrappar@uni-mainz.de

Funding information
CCSG, Grant/Award Number: P30 CA21765; Deutsche Forschungsgemeinschaft (DFG), Grant/Award Number: FR2704/3–1; NIH, Grant/Award Numbers: CA-21765, NS-37956; American Lebanese and Syrian Associated Charities of St. Jude Children's Research Hospital

Abstract

Aims: Nijmegen breakage syndrome (NBS) is a rare autosomal recessive disorder caused by hypomorphic mutations of NBS1. NBS1 is a member of the MRE11-RAD50-NBS1 (MRN) complex that binds to DNA double-strand breaks and activates the DNA damage response (DDR). *Nbs1* inactivation in neural progenitor cells leads to microcephaly and premature death. Interestingly, *p53* homozygous deletion rescues the NBS1-deficient phenotype allowing long-term survival. The objective of this work was to determine whether simultaneous inactivation of *Nbs1* and *p53* in neural progenitors triggered brain tumorigenesis and if so in which category this tumour could be classified.

Methods: We generated a mouse model with simultaneous genetic inactivation of *Nbs1* and *p53* in embryonic neural stem cells and analysed the arising tumours with in-depth molecular analyses including immunohistochemistry, array comparative genomic hybridisation (aCGH), whole exome-sequencing and RNA-sequencing.

Results: NBS1/P53-deficient mice develop high-grade gliomas (HGG) arising in the olfactory bulbs and in the cortex along the rostral migratory stream. In-depth molecular analyses using immunohistochemistry, aCGH, whole exome-sequencing and RNA-sequencing revealed striking similarities to paediatric human HGG with shared features with radiation-induced gliomas (RIGs).

Peter J McKinnon and Pierre-Olivier Frappart equally contributed to this work.

Conclusions: Our findings show that concomitant inactivation of *Nbs1* and *p53* in mice promotes HGG with RIG features. This model could be useful for preclinical studies to improve the prognosis of these deadly tumours, but it also highlights the singularity of NBS1 among the other DNA damage response proteins in the aetiology of brain tumours.

KEYWORDS
genomic rearrangements, high-grade glioma, NBS1, P53, PDGFRA

INTRODUCTION

Genomic instability is a general trait of most cancer cells. In addition to mutations and/or gene amplifications that are an initial requirement for neoplastic transformation, cancer cells exhibit further features of genomic instability, such as chromosomal aberrations and aneuploidy.[1] The functional link between genomic instability and cancer is mirrored by several genomic instability disorders such as Lynch syndrome, Nijmegen breakage syndrome (NBS) and ataxia–telangiectasia (A-T).[2] NBS is an autosomal recessive disorder caused by hypomorphic mutations of NBS1 (also named NBN/Nibrin), which lead to microcephaly and tumour predisposition.[3] NBS1 is required for several essential biological processes including DNA damage response (DDR), DNA replication, DNA repair, cell cycle checkpoint control and apoptosis. NBS patients harbour an increased risk of developing a variety of different malignancies including lymphomas, perianal rhabdomyosarcoma[4–6] and medulloblastoma.[7] Moreover, *NBS1* heterozygous carriers were shown to exhibit a higher risk of developing prostate cancer and ovarian tumours,[8–10] breast cancer,[11–16] melanoma,[17] pancreatic ductal adenocarcinoma,[18,19] and colorectal carcinoma and larynx cancer.[16] *NBS1* polymorphisms were also shown to be associated with increased cancer risk.[20] A variety of different mouse models of NBS have been generated. Null mutation of *Nbs1* causes early in utero lethality at E3.5,[21,22] but *Nbs1* heterozygosity predisposes to tumour development and irradiation-induced tumorigenesis.[22] Mice expressing C-terminal truncated NBS1 survive until adulthood and exhibit many features of NBS including growth retardation and development of thymic lymphomas.[23] However, they fail to mimic the neurological phenotype and brain tumour predisposition. In turn, a conditional deletion model for *Nbs1* in neural progenitors leads to a more severe phenotype compared to NBS patients that include microcephaly, ataxia and premature lethality around 3 weeks of age.[24]

P53 is a master regulator of the DNA damage and cellular stress response. It controls a large number of genes involved in cell cycle arrest, senescence and apoptosis. It eliminates somatic and stem cells that have acquired a certain amount of genomic instability. *p53* inactivation was shown to trigger medulloblastoma formation in several DDR-deficient mice such as BRCA2, XRCC4, LIG4 or XRCC2.[25–27] Previously, it was shown that co-deletion of *p53* substantially rescues the microcephaly phenotype driven by NBS1 loss, but it is currently unknown whether tumorigenesis occurs in this setting.[24] To address this important question, we conditionally deleted *Nbs1* and *p53* in vivo in neural stem cells using *Nestin-Cre*. Remarkably, we found

> **Key Points**
>
> - *Nbs1* and *p53* simultaneous deletion in *Nestin*-positive neural progenitors promotes high-grade glioma.
> - *Nbs1* and *p53* simultaneous inactivation in *Nestin-positive* neural progenitors does not dramatically promote medulloblastoma formation.
> - NBS1/P53-deficient gliomas recapitulate some of the features of human radiation-induced high-grade glioma (RIG).

that simultaneous deletion of these genes led to the formation of high-grade astrocytic tumours typically localised in the olfactory bulbs and cortical region. To a lesser extent, medulloblastomas also arose. Characterisation of the arising tumours showed heterogenous hyperactivation of specific pathways that occur in the human counterpart including PDGFRA. By systematic comparison of NBS1/P53-deficient gliomas with the different human glioma subtypes, we discovered that NBS1/P53-deficient HGG most closely resemble human paediatric HGG, with characteristics of radiation-induced glioma (RIG). These findings are consistent with the function of NBS1 in DDR and the protection of common fragile sites (CFS). Collectively, our data suggest a role for NBS1 in the aetiology of HGG and provide a novel preclinical model to allow a detailed study of this tumour type.

MATERIALS AND METHODS

Mice

The *Nbs1* floxed (B6;129-*Nbs1*^tm1Zqw^), *p53* knock-out (B6.129S2-*P53*^tm1Tyj/J^), *p53* floxed (FVB.129-*P53*^tm1Brn^), *Pten* floxed (B6.129S4-*Pten*^tm1Hwu/J^) were as described.[24] The control group wild type (WT) was composed of *Nbs1*^+/+^; *Nbs1*^+/F^; *Nbs1*^F/F^; *p53*^F/−^; *p53*^F/F^; *p53*^+/−^; *Nbs1*^+/+^, *p53*^F/F^; *Nbs1*^+/+^, *p53*^F/−^; *Nbs1*^+/+^, *p53*^+/−^; *Nbs1*^+/+^, *p53*^F/F^; *Nbs1*^F/F^, *p53*^F/−^; *Nbs1*^F/F^, *p53*^+/−^; *Nbs1*^F/F^, *p53*^F/F^; *Nbs1*^+/F^, *p53*^F/F^; *Nbs1*^+/F^, *p53*^F/−^; *Nbs1*^+/F^, *p53*^+/−^; *Nbs1*^+/F^, *p53*^F/F^. Mice of other experimental groups were identified as follows: *Nbs1*^Nes-Cre^ = *Nbs1*^F/F^, *Nestin-Cre*^+/−^, *p53*^Nes-Cre^ = *p53*^F/−^, *Nestin-Cre*^+/−^ or *p53*^F/F^, *Nestin-Cre*^+/−^; *Nbs1/p53*^Nes-Cre^ = *Nbs1*^F/F^, *p53*^F/−^, *Nestin-Cre*^+/−^ or *Nbs1*^F/F^, *p53*^F/F^, and *Nestin-Cre*^+/−^.

Histology and immunohistochemistry

Brains were collected in 4% (w/v) phosphate-buffered saline (PBS)-paraformaldehyde (PFA) for 24 h at 4°C; 3 μm paraffin sections were performed. Immunohistochemistry included cell conditioning with Ventana (Ventana Medical Systems) cell conditioner 1 for 64 min, pre-primary peroxidase inhibition, incubation with OptiView HQ Universal Linker for 12 min, incubation with OptiView HRP Multimer for 12 min, OptiView Amplification (setting of OptiView Amplifier and OptiView Amplifier Multimer both for 12 min) and incubation with haematoxylin for 4 min each. The following antibodies were used: Anti-γ-H2AX, anti-GFAP (Dako, Z0334), anti-SYN (MRQ-40, Sigma-Aldrich), anti-PTEN (Cell Signaling Technology, #9559), anti-PDGFRA (Santa Cruz, sc-338), anti-CCND1 (92G2, Cell Signaling Technology, #2978), anti-CCND2 (D52F9, Cell Signaling Technology, #3741). The antibody was incubated for 32 min at 37°C. Incubation was followed by Ventana standard signal amplification, UltraWash, counterstaining with one drop of haematoxylin for 4 min, and one drop of bluing reagent for 4 min. For visualisation, the ultraViewUniversal DAB Detection Kit (Ventana) was used. Images were acquired on an Axioplan2 microscope (Carl Zeiss) equipped with an AxioCamHR camera and AxioVision Version 4.8 (both Carl Zeiss) software. TUNEL staining was performed as described.[28] Magnifications are given in figure legends. For TUNEL and γ-H2AX at least five serial sections were counted for each mouse.

Western blot

Tumour tissues were lysed in sodium dodecyl sulftate (SDS) boiling buffer. Samples were denatured at 95°C for 5 min and electrophoretically separated on 4–12% Bis-Tris or 3–8% Tris–Acetate gels (Invitrogen). Proteins were blotted onto nitrocellulose membranes (Life Technologies). After blocking (5% milk powder, 0.05% Tween 20 in PBS) at room temperature for 1 h, the membranes were incubated overnight at 4°C with the primary antibody in blocking solution. The following antibodies were used in human samples: anti-NIBRIN (Sigma, HPA001429, 1:300), anti-RAD50 (Santa Cruz, sc-56209, 1:200), anti-MRE11 (Abcam, 12D7, 1:500), anti- β-ACTIN (Cell Signaling Technology, #4970, 1:1000) and in mouse neural stem cells: anti-NIBRIN (Cell Signaling Technology, #3002, 1:1000), anti-RB1 (Cell Signaling Technology, 4H1, #9309, 1:1000), anti-DICER (Santa Cruz, sc-136979, 1:1000), anti-PTEN (Cell Signaling Technology, #9559, 1:1000), anti-AKT (Cell Signaling Technology, #9272, 1:1000), anti-S6-Ribosomal protein (Cell Signaling Technology, #2271, 1:1000) and anti-β-ACTIN (Cell Signaling Technology, #4970, 1:1000). Incubation with secondary horseradish peroxidase-conjugated anti-mouse or anti-rabbit antibody (Cell Signaling Technology, 1:3000) for 1 h at room temperature was followed by immunodetection with the Western Blotting Detection System (Medac GmbH, Wedel, Germany).

Mouse HGG stem cell line isolation and culture

The isolation and the culture of HGG cell lines were performed using the protocol to isolate and culture neural stem cells described in Frappart et al.[24]

OMIC analysis

Isolation of genomic DNA and array CGH analysis were performed as described.[25] Whole-exome sequencing (WES), panel-sequencing and RNA-sequencing were performed as described.[29–32]

Gene set enrichment analysis (GSEA)

Log2CPM (counts per million reads) was used for gene set enrichment analysis with GSEA version 3.0.[33,34] Specifically, we used '-metric signal2noise -set_min 4 -permute gene_set'. The gene sets used were taken from Verhaak et al[35] and Cahoy et al[36] and describe different glioma subtypes.

HGG and MB databases

The website cBioportal (www.cbioportal.org) was used to identify NBS1, MRE11A, RAD50 and ATM mutations in HGG (2242 patients) and MB (791 patients) using the following studies[37–46] and TCGA Firehose Legacy and PanCancer Atlas. The website St. Jude Cloud PeCan (www.stjude.cloud) was used to determine their mutations in paediatric HGG and MB. NBS1 was found to be mutated in two out of 166 HGG patients and zero out of 693 MB patients; MRE11A was found mutated in three out of 166 HGG patients and zero out of 693 MB patients; RAD50 was found mutated in four out of 166 HGG patients and zero out of 693 MB patients.

Statistical analysis

GraphPad Prism 5 software was used for statistical analysis. A two-tailed t-test was performed as indicated. p-values were based on two-sided tests.

RESULTS

p53 inactivation in Nbs1^Nes-Cre^ brains allows long-term survival

We previously showed that neural stem cell-specific inactivation (via Nestin-cre) of Nbs1 (Nbs1^Nes-Cre^) was lethal by postnatal day 21 (P21) and that this phenotype could be rescued by the concomitant deletion

(A)

(B) *Nbs1^Nes-Cre*   *Nbs1^Nes-Cre, p53^-/-*

(C)

(D) *Nbs1^Nes-Cre*   *Nbs1^Nes-Cre, p53^-/-*

(E)

(F)

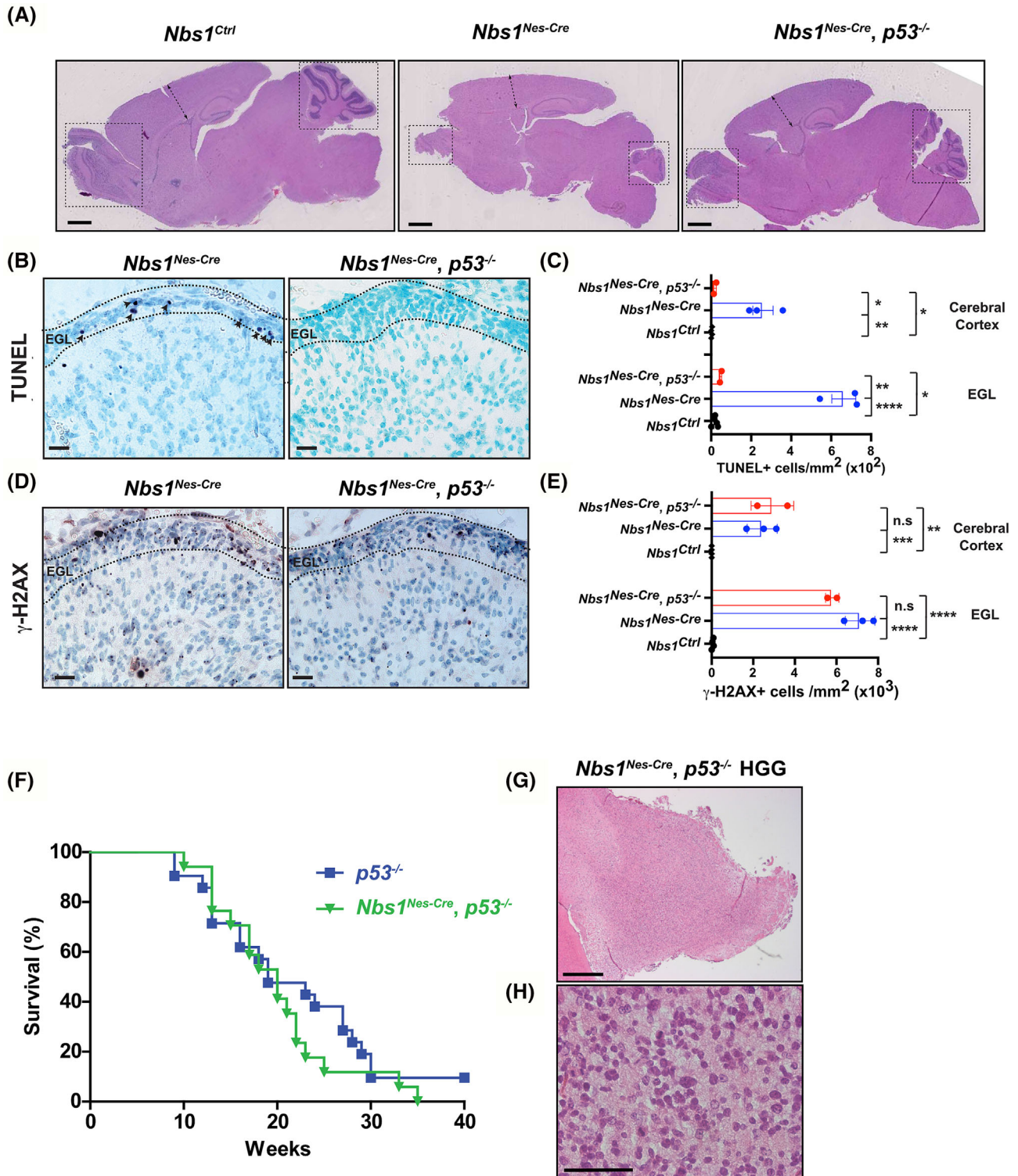**(G)** *Nbs1^Nes-Cre, p53^-/-* HGG

(H)

FIGURE 1 Legend on next page.

of both *p53* alleles leading to long-term survival[24] (Figure 1A). This finding suggested that loss of NBS1 in neural stem cells triggered a p53-dependent damage response leading to cell growth arrest or apoptosis. To dissect the mechanism underlying this rescue, we performed TUNEL staining (Figure 1B,C) and indeed found a significant drop in the number of cells undergoing apoptosis in neuroproliferative regions of the brain, the external granular layer (EGL) and the cerebral cortex. This, in turn, leads to the rescue of the microcephaly phenotype in the cerebellum, cerebral cortex and olfactory bulbs (Figure 1A). We hypothesized that chromosomal instability accumulated due to NBS1 loss, leading to p53-mediated apoptosis as shown previously. Interestingly, the number of γ-H2AX positive cells in *Nbs1*$^{Nes-Cre}$ and *Nbs1*$^{Nes-Cre}$/*p53*$^{-/-}$ brains was unchanged (Figure 1D,E). It is likely, that in the absence of p53 and high-level DNA damage, a senescence mechanism or cell cycle checkpoint would be activated as observed in the NBS1-deficient skin[47] or mouse embryonic fibroblasts (MEF), to prevent the accumulation of DNA damage.

We then monitored these animals for 10 months. However, both the *p53*$^{-/-}$ and *Nbs1*$^{Nes-Cre}$/*p53*$^{-/-}$ mice exhibited premature death, often before 6 months of age and thus limited the use of the *Nbs1*$^{Nes-Cre}$/*p53*$^{-/-}$ mouse model to study tumorigenesis (Figure 1F). Indeed, most of the animals developed lymphoma as previously described for p53-deficient mice. However, 17% of *Nbs1*$^{Nes-Cre}$/*p53*$^{-/-}$ presented with subclinical high-grade astrocytic tumours (Figure 1G,H). Therefore, we performed a conditional gene deletion approach to focus our study on these brain tumours.

NBS1/P53 deficiency predisposes to high-grade gliomas (HGG) and medulloblastoma

To overcome premature lethality, which unfortunately occurred independent of brain tumour development, we generated a cohort of conditional *Nbs1*/*p53*$^{Nes-Cre}$ and respective control mice to monitor them for 10 months. The control groups were composed of WT and *p53*$^{Nes-Cre}$ mice. Statistical analysis showed a significantly decreased survival between *Nbs1*/*p53*$^{Nes-Cre}$ vs WT ($p < 0.0001$) or *p53*$^{Nes-Cre}$ mice ($p = 0.0002$) (Figure 2A). No statistical difference was observed between the survival of WT and *p53*$^{Nes-Cre}$ mice ($p = 0.1805$).

Histopathological analysis of *Nbs1*/*p53*$^{Nes-Cre}$ mice revealed that reduced survival was indeed due to brain tumour development (Figure 2B–D). Overall, tumour incidence was 68% in the *Nbs1*/*p53*$^{Nes-Cre}$ group and the average age at death was 39.7 weeks (Figure 2B). In contrast, only 17% of *p53*$^{Nes-Cre}$ mice displayed brain tumours (Figure 2B). We found most of the tumours in the olfactory bulbs (OB) but also in the cerebral cortex or the cerebellum (Figure 2B,C). Conventional haematoxylin–eosin (H&E) staining for histopathological analysis identified the vast majority of the tumours as gliomas. They developed a fibrillary matrix, had increased nuclear pleomorphism and a subset of multinucleated giant cells and were mitotically active. All these features suggested that they are high-grade astrocytic tumours. In addition, they showed diffuse infiltration of the surrounding brain tissue, and some tumours showed microvascular proliferation and/or necrosis reminiscent of glioblastoma. Further immunophenotyping showed a lack of synaptophysin and low to moderate GFAP immunoreactivity which were associated with poorly differentiated gliomas (classified as HGGs) (Figure 2D). The remaining tumours localised exclusively to the cerebellum and resembled medulloblastoma (Figure 2C). Notably, the medulloblastomas often developed simultaneously with HGG (Figure 2C). In contrast to *Nbs1*/*p53*$^{Nes-Cre}$, the *p53*$^{Nes-Cre}$ mice showed no medulloblastoma formation and the few arising HGG localised to the cerebral cortex, and spared the olfactory bulb (Figure 2B). Furthermore, systematic comparison of cortical HGG in both genotypes did not reveal any histological differences either in terms of grading or in proliferative capacity.

Mutations of *NBS1*, *RAD50* and *MRE11A* are extremely rare events in human HGG

Our findings were consistent with several reports showing that *NBS1* mutations associated with *P53* mutations were found in a very small subgroup of human HGG and medulloblastomas.[48,49] To explore this further, we analysed several databases and tumour samples at our disposal to determine whether the *NBS1* and *P53* status could define a subtype of tumours and could be used as biomarkers. Surprisingly, in contradiction to former studies, cancer mutations databases such as cBioPortal (www.cbioportal.org) or the Paediatric Cancer Genome Project (www.stjude.cloud) did not list many *NBS1*, *RAD50* and

FIGURE 1 *P53* inactivation rescues *Nbs1*$^{Nes-Cre}$ deleterious brain phenotype. (A) Rescue of *Nbs1*$^{Nes-Cre}$ brain defects at P21 by *p53* inactivation. (B) Lack of apoptosis in *Nbs1*$^{Nes-Cre}$, *p53*$^{-/-}$ EGL and cerebral cortex compared to *Nbs1*$^{Nes-Cre}$ EGL and cerebral cortex. Scale bars = 20 μM. (C) the number of TUNEL-positive cells in EGL of *Nbs1*$^{Nes-Cre}$, *p53*$^{-/-}$ brains is significantly reduced compared to the ones of *Nbs1*$^{Nes-Cre}$ brains. *Nbs1*$^{Nes-Cre}$ (N = 3), *Nbs1*$^{Nes-Cre}$, *p53*$^{-/-}$ (N = 2), *Nbs1*^{Ctrl} (N = 4). *Nbs1*$^{Nes-Cre}$ vs *Nbs1*^{Ctrl} (cerebral cortex **:$p = 0.0018$, EGL ****:$p < 0.0001$), *Nbs1*$^{Nes-Cre}$, *p53*$^{-/-}$ vs *Nbs1*$^{Nes-Cre}$ (cerebral cortex *: $p = 0.0359$, EGL **:$p = 0.0042$), *Nbs1*$^{Nes-Cre}$, *p53*$^{-/-}$ vs *Nbs1*^{Ctrl} (cerebral cortex *:$p = 0,0181$, EGL *:$p = 0.0360$). (D) both *Nbs1*$^{Nes-Cre}$ and *Nbs1*$^{Nes-Cre}$, *p53*$^{-/-}$ EGL exhibit γ-H2AX foci. Scale bars = 20 μM. (E) Quantification of γ-H2AX + cells in *Nbs1*$^{Nes-Cre}$ and *Nbs1*$^{Nes-Cre}$, *p53*$^{-/-}$ EGL and cerebral cortex. N.s: no significant differences. *Nbs1*$^{Nes-Cre}$ (N = 3), *Nbs1*$^{Nes-Cre}$, *p53*$^{-/-}$ (N = 2), *Nbs1*^{Ctrl} (N = 4). *Nbs1*$^{Nes-Cre}$ vs *Nbs1*^{Ctrl} (cerebral cortex ***:$p = 0.0009$, EGL ****:$p < 0.0001$), *Nbs1*$^{Nes-Cre}$, *p53*$^{-/-}$ vs *Nbs1*$^{Nes-Cre}$ (cerebral cortex: non-significant (n.s), EGL: non-significant (n.s)), *Nbs1*$^{Nes-Cre}$, *p53*$^{-/-}$ vs *Nbs1*^{Ctrl} (cerebral cortex **: $p = 0.0027$, EGL ****:$p < 0.0001$). (F) Survival curves of *p53*$^{-/-}$ (N = 22) and *Nbs1*$^{Nes-Cre}$, *p53*$^{-/-}$ (N = 18) mice. No significant differences between the survival of *p53*$^{-/-}$ and *Nbs1*$^{Nes-Cre}$, *p53*$^{-/-}$ mice. Representative HGG in *Nbs1*$^{Nes-Cre}$, *p53*$^{-/-}$ brains. Magnification ×25, scale bars = 600 μM (G) and ×400, scale bars = 60 μM (H).
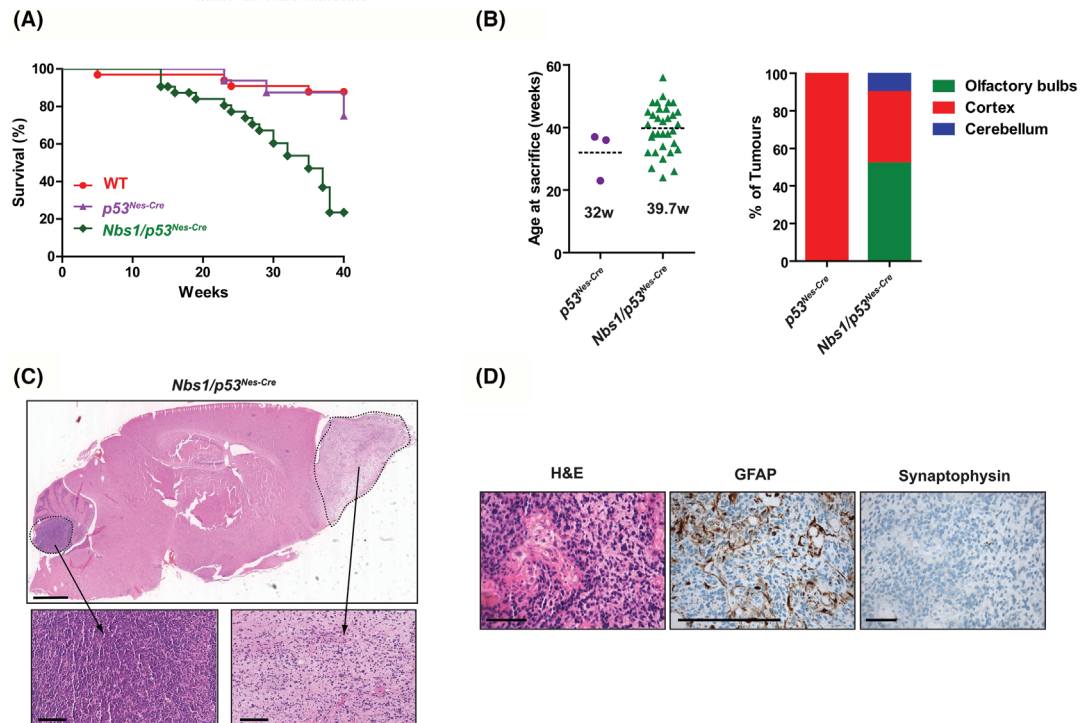
FIGURE 2 *Nbs1/p53^Nes-Cre* mice develop high-grade gliomas and medulloblastoma. (A) Survival curves of WT ($N = 39$), $p53^{-/-}$ ($N = 18$) and *Nbs1/p53^Nes-Cre* ($N = 51$). Survival comparison: WT vs $p53^{Nes-Cre}$ (non-significant, n.s), WT vs *Nbs1/p53^Nes-Cre* ($p < 0.0001$), $p53^{Nes-Cre}$ vs *Nbs1/p53^Nes-Cre*, ($p = 0.0002$). (B) Comparison of the age at death between $p53^{Nes-Cre}$ ($N = 3$) and *Nbs1/p53^Nes-Cre* ($N = 33$) mice, n.s: non-significant, and localization of the tumours in $p53^{Nes-Cre}$ and *Nbs1/p53^Nes-Cre* mice. (C) Representative HGG and medulloblastoma from *Nbs1/p53^Nes-Cre* mice. Brain (scale bar = 1 mm), Medulloblastoma and glioma (scale bars = 100 μM) (D) immunohistochemistry of HGG from *Nbs1/p53^Nes-Cre*: H&E straining (scale bar = 80 μM), GFAP staining (scale bar = 200 μM), Synaptophysin staining (scale bar 60 μM).

MRE11A mutations in paediatric and adult brain tumours (Figure 3A). Indeed, mutations of *RAD50*, *NBS1* and *MRE11A* are found, depending on their types, in fewer than 1% of the tumours.

To get a deeper insight, we first decided to analyse at the protein level 50 primary human adult HGG samples. Interestingly, we found that some of the HGGs exhibited depletion of RAD50, NBS1 or MRE11 (Figure 3B). We were able to perform panel sequencing on seven of these MRN-deficient tumours (Figure 3C). However, mutations/polymorphisms of *NBS1*, *RAD50* or *MRE11A* were found in only two out of the seven sequenced tumours (*NBS1* 0/7, *RAD50* 1/7 and *MRE11A* 1/7) suggesting that mutations of the MRN complex genes are extremely rare in HGG. This result is consistent with the database of cancer mutations. Altogether, these data confirmed the rarity of mutations in *NBS1*, *RAD50* and *MRE11A* in both adult and paediatric human HGG. Nevertheless, our data indicate that a non-negligible percentage of HGG exhibit lower levels of MRN proteins.

Immunohistochemical (IHC) characterisation of NBS1/P53-deficient HGG

To determine the classification of the *Nbs1/p53^Nes-Cre*, an IHC analysis was performed using well-known markers of the RTK (receptor tyrosine kinase), NTRK (neurotrophic tropomyosin–receptor kinase), p53

and RB1 pathways known to be HGG drivers (Figure 4A). The semi-quantitative measurement of the staining was performed on 13 HGG by a neuropathologist. A value of 0 was given for lack of expression (basal expression in WT brain tissue) and values of 1–4 for increasing expression. PDGFRA (Figure 4B) and phosphorylated-Met (p-Met) (Figure 4C) were detectable in 10 out of 13 tumours (76%), CCND1 (Figure 4D) and CCND2 (Figure 4E) were found in eight out of 13 (62%) and six out of 13 (46%), respectively. Notably, all 13 tumours overexpressed at least one of these oncogenes. In addition, we observed partial or total depletion of PTEN (Figure 4F) in five out of 13 tumours (38%). PTEN depletion was often associated with the up-regulation of phosphorylated-RPS6 (p-RPS6) (Figure 4H). Finally, *Dicer1* another tumour suppressor was lost in three out of 13 tumours (23%) (Figure 4G). In parallel, western blot analysis on mouse *Nbs1/p53^Nes-Cre* HGG spheroid cell lines showed depletion of Rb1, Dicer1, Akt1, Pten and up-regulation of p-RPS6 consistently with IHC data (Figure 4I).

NBS1/P53-deficient HGG exhibit multiple genomic rearrangements

An array comparative genome hybridization (aCGH) analysis was performed in glioma tissue of this genotype to uncover chromosomal
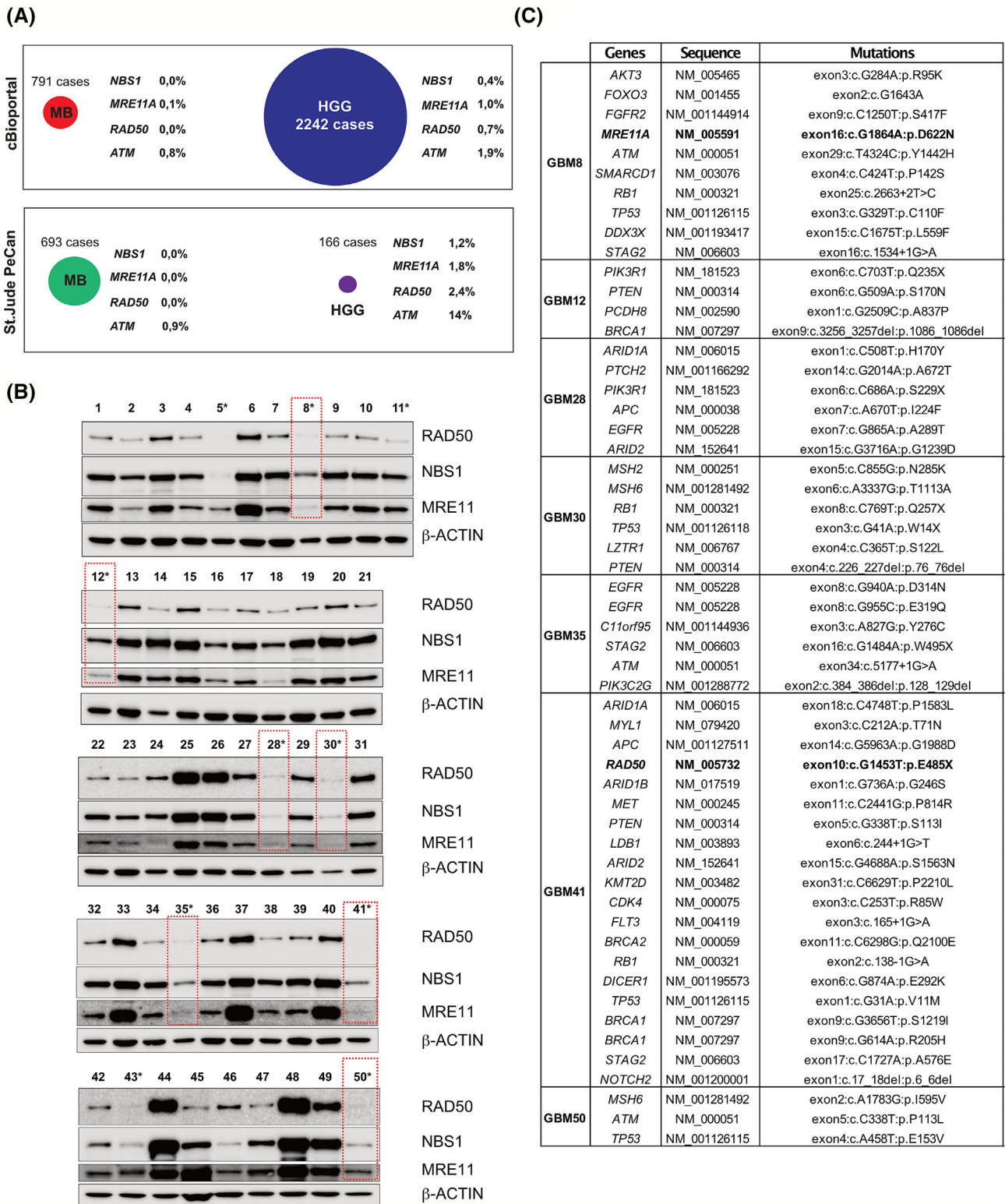
FIGURE 3 Expression of NBS1, RAD50 and MRE11A in human HGG. (A) Summary of *NBS1*, *MRE11A*, *RAD50* and *ATM* genetic alterations in paediatric and adult HGG in cBioPortal and St. Jude PeCan databases. (B) Western-blot analysis of 50 primary human HGG indicates various levels of expression of NBS1 (95 kDa), RAD50 (163 kDa) and MRE11 (81 kDa). (C) Panel sequencing of the primary HGGs exhibiting a low level of RAD50, NBS1 and MRE11. Only one HGG exhibits a truncating *RAD50* mutation and another HGG shows a *MRE11A* variant which was not reported as pathogenic.
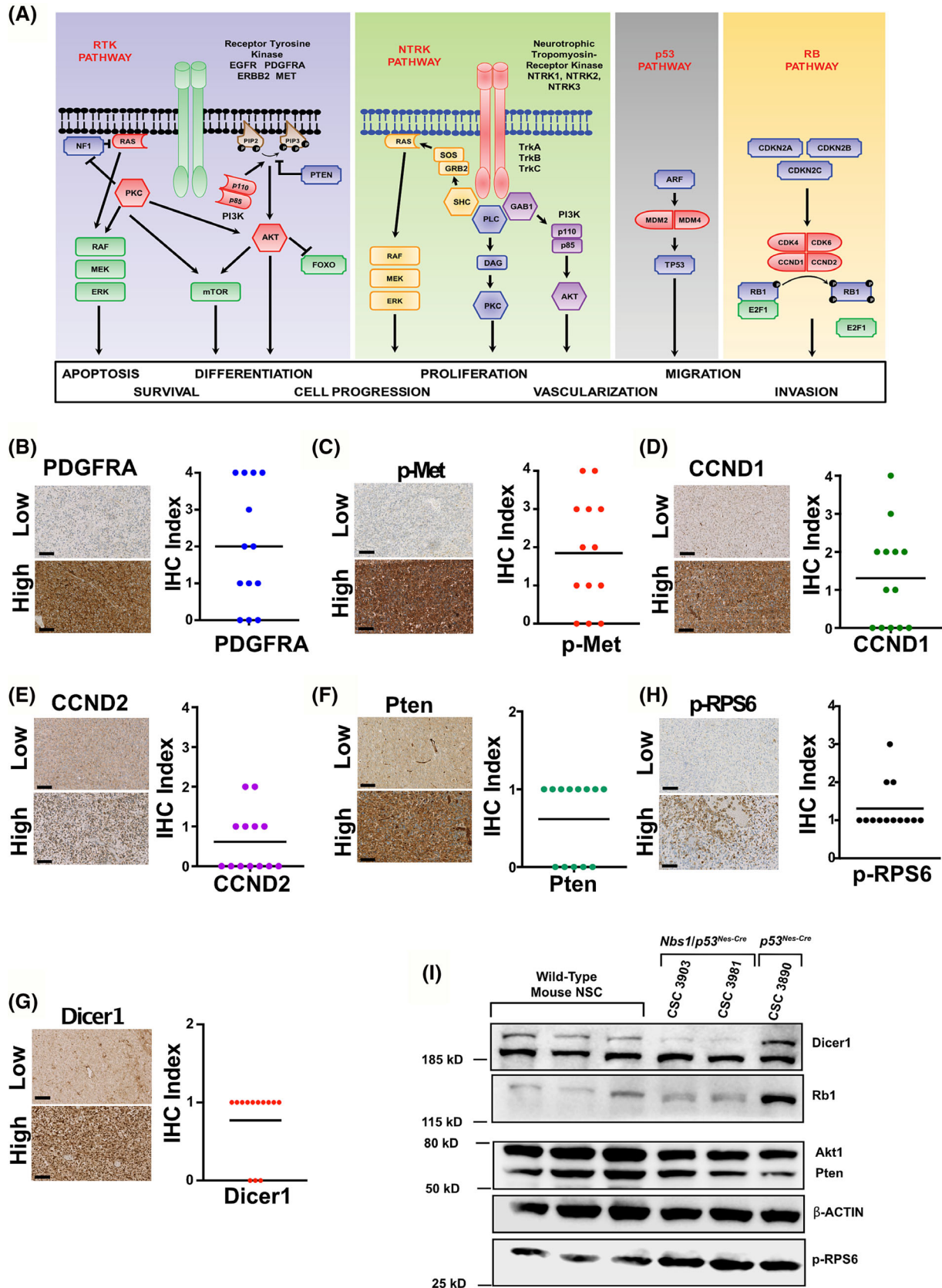
(C)

	Genes	Sequence	Mutations
GBM8	AKT3	NM_005465	exon3:c.G284A:p.R95K
	FOXO3	NM_001455	exon2:c.G1643A
	FGFR2	NM_001144914	exon9:c.C1250T:p.S417F
	MRE11A	**NM_005591**	**exon16:c.G1864A:p.D622N**
	ATM	NM_000051	exon29:c.T4324C:p.Y1442H
	SMARCD1	NM_003076	exon4:c.C424T:p.P142S
	RB1	NM_000321	exon25:c.2663+2T>C
	TP53	NM_001126115	exon3:c.G329T:p.C110F
	DDX3X	NM_001193417	exon15:c.C1675T:p.L559F
	STAG2	NM_006603	exon16:c.1534+1G>A
GBM12	PIK3R1	NM_181523	exon6:c.C703T:p.Q235X
	PTEN	NM_000314	exon6:c.G509A:p.S170N
	PCDH8	NM_002590	exon1:c.G2509C:p.A837P
	BRCA1	NM_007297	exon9:c.3256_3257del:p.1086_1086del
GBM28	ARID1A	NM_006015	exon1:c.C508T:p.H170Y
	PTCH2	NM_001166292	exon14:c.G2014A:p.A672T
	PIK3R1	NM_181523	exon6:c.C686A:p.S229X
	APC	NM_000038	exon7:c.A670T:p.I224F
	EGFR	NM_005228	exon7:c.G865A:p.A289T
	ARID2	NM_152641	exon15:c.G3716A:p.G1239D
GBM30	MSH2	NM_000251	exon5:c.C855G:p.N285K
	MSH6	NM_001281492	exon6:c.A3337G:p.T1113A
	RB1	NM_000321	exon8:c.C769T:p.Q257X
	TP53	NM_001126118	exon3:c.G41A:p.W14X
	LZTR1	NM_006767	exon4:c.C365T:p.S122L
	PTEN	NM_000314	exon4:c.226_227del:p.76_76del
GBM35	EGFR	NM_005228	exon8:c.G940A:p.D314N
	EGFR	NM_005228	exon8:c.G955C:p.E319Q
	C11orf95	NM_001144936	exon3:c.A827G:p.Y276C
	STAG2	NM_006603	exon16:c.G1484A:p.W495X
	ATM	NM_000051	exon34:c.5177+1G>A
	PIK3C2G	NM_001288772	exon2:c.384_386del:p.128_129del
GBM41	ARID1A	NM_006015	exon18:c.C4748T:p.P1583L
	MYL1	NM_079420	exon3:c.C212A:p.T71N
	APC	NM_001127511	exon14:c.G5963A:p.G1988D
	RAD50	**NM_005732**	**exon10:c.G1453T:p.E485X**
	ARID1B	NM_017519	exon1:c.G736A:p.G246S
	MET	NM_000245	exon11:c.C2441G:p.P814R
	PTEN	NM_000314	exon5:c.G338T:p.S113I
	LDB1	NM_003893	exon6:c.244+1G>T
	ARID2	NM_152641	exon15:c.G4688A:p.S1563N
	KMT2D	NM_003482	exon31:c.C6629T:p.P2210L
	CDK4	NM_000075	exon3:c.C253T:p.R85W
	FLT3	NM_004119	exon3:c.165+1G>A
	BRCA2	NM_000059	exon11:c.C6298G:p.Q2100E
	RB1	NM_000321	exon2:c.138-1G>A
	DICER1	NM_001195573	exon6:c.G874A:p.E292K
	TP53	NM_001126115	exon1:c.G31A:p.V11M
	BRCA1	NM_007297	exon9:c.G3656T:p.S1219I
	BRCA1	NM_007297	exon9:c.G614A:p.R205H
	STAG2	NM_006603	exon17:c.C1727A:p.A576E
	NOTCH2	NM_001200001	exon1:c.17_18del:p.6_6del
GBM50	MSH6	NM_001281492	exon2:c.A1783G:p.I595V
	ATM	NM_000051	exon5:c.C338T:p.P113L
	TP53	NM_001126115	exon4:c.A458T:p.E153V

FIGURE 4 Legend on next page.

deletions and amplifications. In six HGGs from *Nbs1/p53*^{Nes-Cre} mice, numerous recurrent genomic rearrangements including segmental and total amplifications of chromosomes (Chr) 3, 4 and 5, and recurrent Chr9, Chr12, Chr14 and Chr18 loss were detected in both cortical and olfactory bulb tumours (Figure 5A). To identify specific chromosomal loss and/or gain hot spots, we performed an analysis of altered probes specifically on chromosomes 3, 4, 5, 9, 12, 14 and 18. We focused our analysis on the genes altered in more than four out of six tumours. Unfortunately, except for a few genes that were already found in rare cases of human HGG such as *Dcc* and *Pcdh9*, no systematic specific or recurrent alterations of HGG driver genes were identified (Figure 5B). However, since we already found by IHC and western blot that the RB, RTK, NTRK and AKT pathways were dysregulated, we decided to specifically investigate those (Figure 5C–F). As expected, all these four pathways were disrupted in these gliomas either by amplification of oncogenes or loss of key tumour suppressor genes. Indeed, we found that *Rb1* localised on Chr14 was frequently lost (Figure 5C). In addition, the *Ccnd1*, *Ccnd2* and *Cdk6* genomic loci were amplified in 67% (4/6) and 50% (3/6), respectively, of the HGGs (Figure 5C). *Cdkn2a/b* was altered (gain or loss) in 50% of the HGGs. Similarly, in the AKT pathway, *Akt1* (Chr18) was altered in 100% (6/6) of the HGGs (Figure 5D). *Pten*, was altered in one-third of the gliomas (2/6) similar to what was found by IHC. Nevertheless, AKT1 despite a recurrent loss of one allele, seems to be expressed in *Nbs1/p53*^{Nes-Cre} (Figure 4I). In contrast, *Pten* genomic loss was associated with complete or partial expression loss in at least one-third of the tumours. Consistent with this hypothesis, heterozygous inactivation of *Pten* accelerated HGG development in *Nbs1/p53*^{Nes-Cre} mice (Supplementary Figure 1A,B) but without medulloblastoma formation (Supplementary Figure 1C). In addition to *Pdgfra* and *Egfr*, amplifications of the *Nras* and *Kras* genomic loci were also found in 67% (4/6) of the tumours (Figure 5E). Finally, *Ntrk1* and *Ntrk3* loci were amplified in 50% (3/5) of the HGG analysed (Figure 5F), and in fact, five out of six HGG exhibited amplification of either *Ntrk1* or *Ntrk3*.

In order to identify the tumour suppressor genes localised on Chr9, 12, 14 and 18, tumour exome sequencing was performed on one *Nbs1/p53*^{Nes-Cre} HGG. As expected, we observed similar chromosome loss as those found in aCGH (Figure 5G). However, very few exonic point mutations were found, among them, *Nf1* (Chr11), which may play a role in gliomas (Figure 5H). Similarly, it was not possible to

find small sporadic exonic deletions or insertions and even careful checking at heterozygote germline mutations and small deletions that could become homozygote upon one chromosome loss, did not reveal major findings on Chr9, Chr12, Chr14 and Chr18. Similar results were obtained by sequencing one *Nbs1/p53*^{Nes-Cre}, *Pten*^{+/F} HGG (Supplementary Figure 1D,E). In conclusion, despite recurrent deletions and chromosome loss in *Nbs1/p53*^{Nes-Cre} HGG, we could not find any evidence of systematic genomic inactivation of tumour suppressor genes. However, *Nbs1/p53*^{Nes-Cre} HGG exhibit recurrent events including disruption of the RB, p53, RTK and NTRK pathways with overexpression of PDGFRA, Met, CCND1 and CCND2.
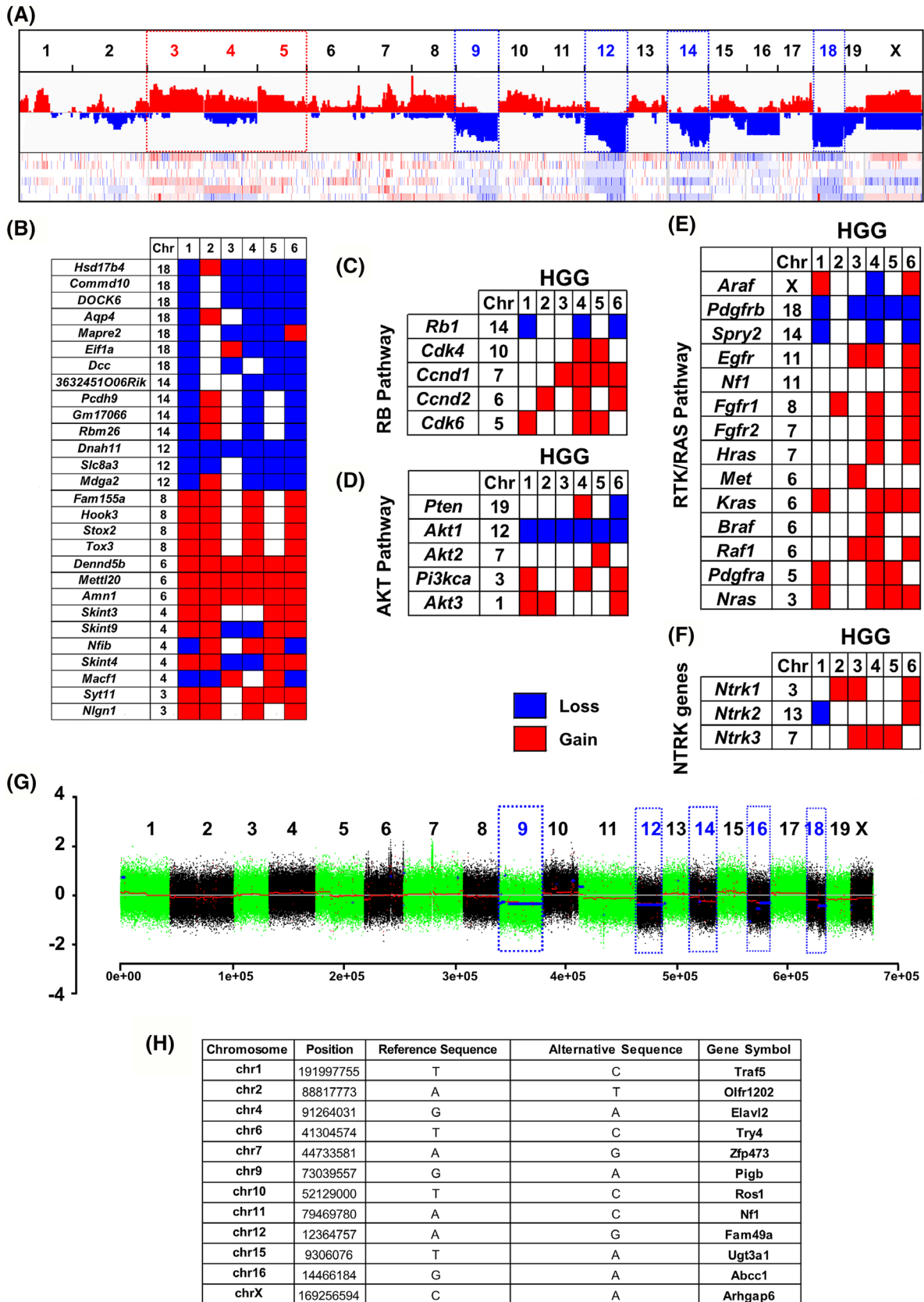
To complement the genomic and IHC data, RNA-sequencing of four HGGs was performed to identify putative activating fusions using the STAR-Fusion algorithm. We focused more specifically on gene fusions such as *ETV6::NTRK* that were already shown in human HGG. However, no common fusion signature was identified. Noticeably, several putative fusions involving FGFR2 and JAK1 were found in three of the HGG (Supplementary Figure 2). However, the fusions seem to be the result of the higher genomic instability of the NBS1-deficient HGG rather than key drivers/markers of the tumour development.

Taken together, the IHC and genomic data indicate that NBS1/P53 deficiency does not trigger a specific sequential inactivation of genes as was formerly observed in DDR-deficient medulloblastoma, but a more heterogeneous and complex set of gene alteration leading to disruption or up-regulation of glioma-associated biological pathways.

Expression-based characterisation of *Nbs1/p53*^{Nes-Cre} HGG

We performed a gene expression comparison between four *Nbs1/p53*^{Nes-Cre} HGG and a cohort of six, *p53*^{Nes-Cre} spontaneous HGG. Interestingly, the heat map based on the 50 top hits of both HGG suggested that *Nbs1/p53*^{Nes-Cre} and *p53*^{Nes-Cre} HGG represent two different entities (Figure 6A). Further analysis by gene set enrichment (GSEA) using glioblastoma signatures from Cahoy et al[36] and Verhaak et al[50] reveals that *Nbs1/p53*^{Nes-Cre} HGG show enriched expression of classical glioblastoma (Figure 6B,C), astrocytic (Figure 6D,E),

---

FIGURE 4 Immunohistochemistry and western blot analysis of the *Nbs1/p53*^{Nes-Cre} –HGGs. (A) Graphical abstract of the main biological pathways known to be altered in HGG. (B) PDGFRA IHC staining in HGG, representative HGG with high or low expression of PDGFRA. (C) Semi-quantitative measurement of PDGFRA expression in 13 *Nbs1/p53*^{Nes-Cre} –HGGs. (D) p-met IHC staining in HGG, representative HGG with high or low expression of p-met. (E) Semi-quantitative measurement of p-met expression in 13 *Nbs1/p53*^{Nes-Cre} –HGGs. (F) CCND1 IHC staining in HGG, representative HGG with high or low expression of CCND1. (G) Semi-quantitative measurement of CCND1 expression in 13 *Nbs1/p53*^{Nes-Cre} –HGGs. (H) CCND2 IHC staining in HGG, representative HGG with high or low expression of CCND2. (I) Semi-quantitative measurement of CCND2 expression in 13 *Nbs1/p53*^{Nes-Cre} –HGGs. (J) Pten IHC staining in HGG, representative HGG with high or low expression/loss of Pten. (K) Semi-quantitative measurement of Pten expression in 13 *Nbs1/p53*^{Nes-Cre} –HGGs. *Pten* seems to be lost in 5 out of 13 HGGs. (L) p-RPS6 IHC staining in HGG, representative HGG with high or low expression of p-RPS6. (M) Semi-quantitative measurement of p-RPS6 expression in 13 *Nbs1/p53*^{Nes-Cre} –HGGs. (N) Dicer1 IHC staining in HGG, representative HGG with high or low expression of p-RPS6. (O) Semi-quantitative measurement of Dicer1 expression in 13 *Nbs1/p53*^{Nes-Cre} –HGGs scale bars = 100 μM. (P) Western-blot analysis of mouse *Nbs1/p53*^{Nes-Cre} HGG spheroids showing depletion of Dicer1, Rb1 and Pten.

(A)

(B)

(C)

RB Pathway — HGG

	Chr	1	2	3	4	5	6
Rb1	14						
Cdk4	10						
Ccnd1	7						
Ccnd2	6						
Cdk6	5						

(D)

AKT Pathway — HGG

	Chr	1	2	3	4	5	6
Pten	19						
Akt1	12						
Akt2	7						
Pi3kca	3						
Akt3	1						

(E)

RTK/RAS Pathway — HGG

	Chr	1	2	3	4	5	6
Araf	X						
Pdgfrb	18						
Spry2	14						
Egfr	11						
Nf1	11						
Fgfr1	8						
Fgfr2	7						
Hras	7						
Met	6						
Kras	6						
Braf	6						
Raf1	6						
Pdgfra	5						
Nras	3						

(F)

NTRK genes — HGG

	Chr	1	2	3	4	5	6
Ntrk1	3						
Ntrk2	13						
Ntrk3	7						

■ Loss
■ Gain

(G)

(H)

Chromosome	Position	Reference Sequence	Alternative Sequence	Gene Symbol
chr1	191997755	T	C	Traf5
chr2	88817773	A	T	Olfr1202
chr4	91264031	G	A	Elavl2
chr6	41304574	T	C	Try4
chr7	44733581	A	G	Zfp473
chr9	73039557	G	A	Pigb
chr10	52129000	T	C	Ros1
chr11	79469780	A	C	Nf1
chr12	12364757	A	G	Fam49a
chr15	9306076	T	A	Ugt3a1
chr16	14466184	G	A	Abcc1
chrX	169256594	C	A	Arhgap6

FIGURE 5 Legend on next page.

mesenchymal (Supplementary Figure 3A,B) and MYC pathway (Supplementary Figure 3C,D) genes. These data are consistent with the genomic ones that suggested a mixed lineage and increased tumour heterogeneity of the *Nbs1/p53*[Nes-Cre] HGG.

DISCUSSION

To characterise the function of NBS1 in the aetiology of brain tumours, we conditionally inactivated it together with *p53*, throughout the nervous system using *Nestin-Cre*. We found a high incidence of HGG development. These HGGs recapitulated the vast majority of the features of human HGG and recurrent biological pathway alterations. Our findings suggested that the key events upon p53 loss are the up-regulation of PDGFRA and other oncogenic factors such as Met and CCND2. The *Nbs1/p53*[Nes-Cre] HGG resemble most of the paediatric HGG subgroup 'pedRTK1' with shared features of RIGs.

It has been shown that concomitant inactivation of DDR genes such as *Brca2*,[27] *Lig4*,[25] *Xrcc2*,[25] *Xrcc4*[26] and *p53* using *Nestin-Cre* triggered medulloblastoma formation originating from granule cells with an incidence of 100% by 6 months of age, indicating a particular requirement for those proteins and DNA repair pathways during cerebellar granule cell development. Surprisingly, the *Nbs1/p53*[Nes-Cre] mice developed very few medulloblastomas that exhibit the DDR-associated SHH signature but mainly HGG, indicating discrepancies between NBS1 and the other DDR proteins. Several arguments could be provided to explain this phenomenon. First, it was shown that apoptosis and cell proliferation induced by double-strand breaks (DSBs) resulting from *Nbs1* inactivation during embryonic development were differentially regulated in the neocortex and the cerebellum by the P53/haematopoietic zinc finger (HZF) complex.[51] Second, it is likely that similar to the skin,[47] the numerous DSB and P53 depletion in NBS1-deficient granule cells would trigger the enhancement of a pro-inflammatory phenotype that may compensate for the lack of apoptosis by blocking cell cycle progression and eliminating damaged cells,[52] whereas in the subventricular zones of the cortex, either the lack of a pro-inflammatory phenotype or its effect on promoting the proliferation of certain cell types or preventing their differentiation would lead to tumour development. Finally, recently it was found in an SHH-medulloblastoma model that complete deletion of *Nbs1* prevented, whereas heterozygous deletion promoted, SHH-MB development.[53]

The literature contains contradictory data on NBS1 mutations in brain tumours. Indeed, homozygous and heterozygous germ-line *NBS1* mutations were shown to predispose to medulloblastoma and gliomas.[7,54–56] However, *Nbs1* heterozygous mice or with hypomorphic mutations[22,23,57,58] do not exhibit brain tumour predisposition suggesting physiologic and genetic discrepancies in the aetiology of brain tumours between humans and mice. Moreover, initial studies reported relatively frequent *NBS1* mutations and polymorphisms associated with *P53* mutations in sporadic medulloblastomas and gliomas.[48,49] Nevertheless, cancer genomic projects and our human findings list only seldom sporadic mutations of *NBS1*, *MRE11A* and *RAD50* in paediatric or adult HGG and medulloblastomas.

The *Nbs1/p53*[Nes-Cre] HGGs are reminiscent of the majority of the genetically engineered mouse models of gliomas based on *p53*, *Pten*, *Nf1* or *Rb1* inactivation.[59,60] However, in contrast to other models, our model exhibits a more pronounced olfactory bulb location that could reflect the cell of origin for this tumour entity.[61] The molecular signature with *PDGFRA* amplification and *P53* mutations and the embryonic pattern is reminiscent of paediatric HGG without H3 and IDH– mutations. However, *Nbs1/p53*[Nes-Cre] HGGs failed to fully recapitulate molecular and genetic characteristics of paediatric HGG.[62–64] Nevertheless, recent studies that focused their work on secondary gliomas arising upon therapeutic radiation also known as RIG were able to provide comprehensive molecular profiling of this tumour entity and a new perspective for the *Nbs1/p53*[Nes-Cre] HGG model.[65–68] Indeed, RIGs cluster with the paediatric receptor tyrosine kinase 1 (pedRTK1) methylation group and exhibit frequent *P53* and *CDKN2A/B* loss together with *PDGFRA*, *MET* and *CDK4* amplifications.[65,66] In addition, an expression-based signature of RIG defined two sub-groups: group A (proneural GBM, MYC pathway up-regulation) and group B (mesenchymal GBM, high mutation burden, decreased DNA repair).[65] All the characteristics of 'mesenchymal GBM' and 'decreased DNA repair' resemble closely those of the *Nbs1/p53*[Nes-Cre] HGGs. These findings are consistent with the reported role of both NBS1 and P53 in preventing radiation-induced tumours. Indeed, it was shown that heterozygous inactivation of *p53* together with *Pten* triggers gliomas upon radiation with multiple genomic rearrangements including recurrent *Met* amplification.[69,70] Similarly, *Nbs1* heterozygote mice upon irradiation developed multiple tumours including thyroid but surprisingly no brain tumours.[22] The lack of brain tumours in *Nbs1* heterozygote irradiated mice may be explained by the advanced age of the mice at the time of irradiation. Moreover, the genetic alterations observed in RIG were shown to be associated with chromosomal fragile sites[71,72] and NBS1 is involved in the processing of those sites.[73] However, we cannot exclude that the overall high genomic instability observed in *Nbs1/p53*[Nes-Cre] is also due to the role of NBS1 in DNA replication[74,75] and DSB DDR.[76]

FIGURE 5 Recurrent genomic rearrangements in *Nbs1/p53*[Nes-Cre] HGG. (A) Summary of the aCGH analysis of six *Nbs1/p53*[Nes-Cre] –HGGs reveals recurrent chromosomes (Chr) 3, 4, 5 amplification and Chr 9, 12, 14 and 18 loss. Summary of the genomic rearrangements by aCGH affecting the RB1 (B), AKT1 (C), RTK/RAS (D) and NTRK (E) pathways in the *Nbs1/p53*[Nes-Cre] HGGs. Each column represents a single tumour, and each row a gene. Each red square indicates a genomic amplification whereas blue squares indicate a genomic loss. (1) HGG #1776, (2) HGG #1855, (3) HGG #2117, (4) HGG #2069, (5) HGG #2185, (6) HGG #2274. Whole-exome sequencing of *Nbs1/p53*[Nes-Cre] HGG. (F) Exome-sequencing of HGG#2117. (G) Point mutations summary in HGG#2117.
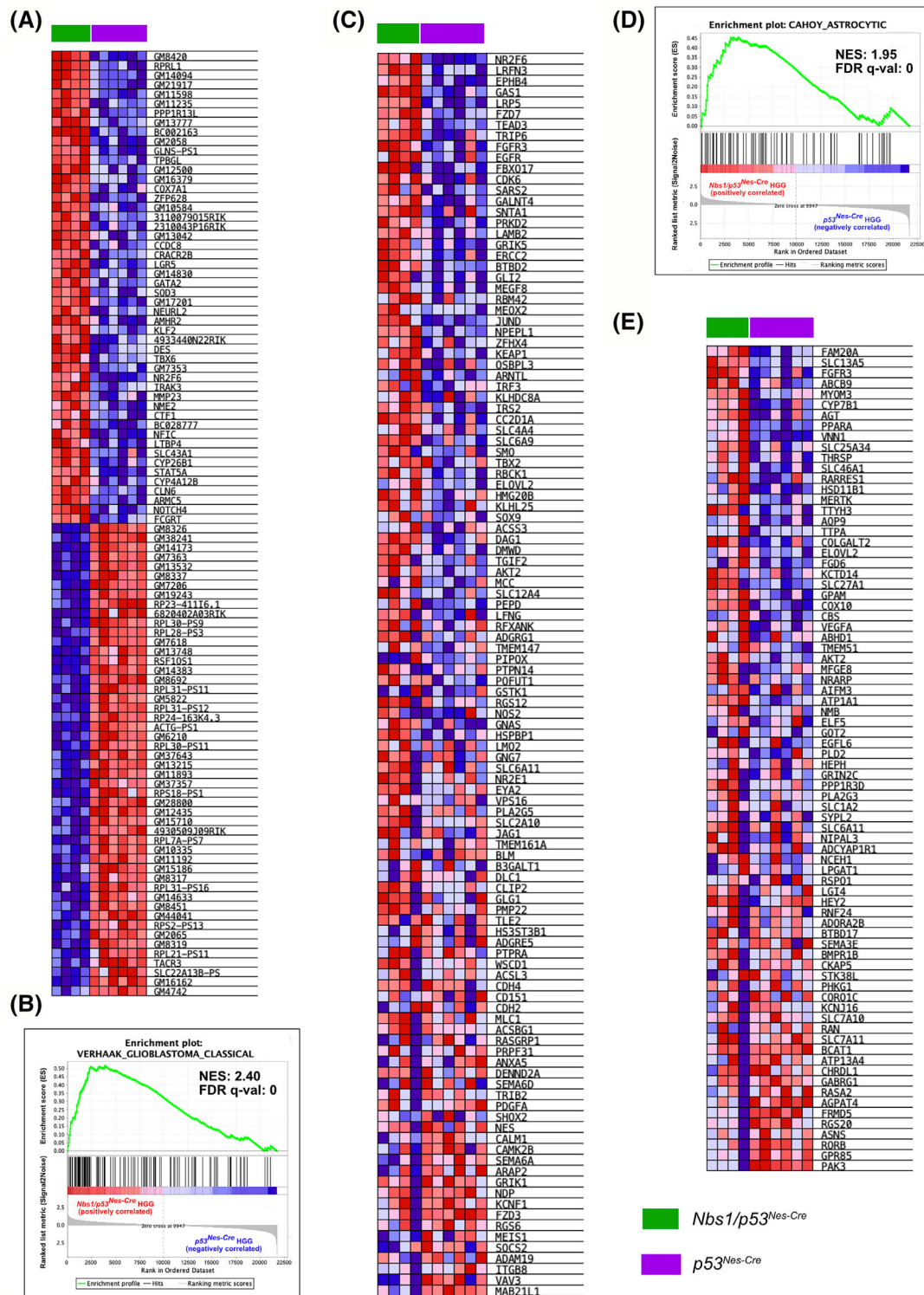
FIGURE 6 RNA-seq expression profile of *Nbs1/p53^Nes-Cre* vs *p53^Nes-Cre* HGG. (A) Heat map of the 50 top hits differentially expressed genes in *Nbs1/p53^Nes-Cre* (N = 4) vs *p53^Nes-Cre* (N = 6) HGG. (B) GSEA of classical glioblastoma genes set in *Nbs1/p53^Nes-Cre* (N = 4) vs *p53^Nes-Cre* (N = 6). (C) Heat map of the classical glioblastoma genes set differentially expressed in *Nbs1/p53^Nes-Cre* (N = 4) vs *p53^Nes-Cre* (N = 6) HGG. (D) GSEA of an astrocytic gene set in *Nbs1/p53^Nes-Cre* (N = 4) vs *p53^Nes-Cre* (N = 6). (E) Heat map of an astrocytic gene set differentially expressed in *Nbs1/p53^Nes-Cre* (N = 4) vs *p53^Nes-Cre* (N = 6) HGG.

In summary, our study provides a comprehensive analysis of the role of NBS1 in the aetiology of paediatric HGG/RIG and the molecular signatures that accompany the development of these HGG.

AUTHOR CONTRIBUTIONS

Conception and design: David E. Reuss, Peter J. McKinnon and Pierre-Olivier Frappart. Development of methodology: David E. Reuss and Pierre-Olivier Frappart. Acquisition of data (provided animals, acquired and managed patients, provided facilities, etc.): David E. Reuss, Susanna M. Downing, Cristel V. Camacho, Zhao-Qi Wang, Yong-Dong Wang, Andreas von Deimling, Christel Herold-Mende, Peter J. McKinnon and Pierre-Olivier Frappart. Analysis and interpretation of data (e.g., statistical analysis, biostatistics, computational analysis): Susanna M. Downing, Cristel V. Camacho, Yong-Dong Wang, Felix Sahm, Rosario M. Piro, David E. Reuss and Pierre-Olivier Frappart. Writing, review, and/or revision of the manuscript: David E. Reuss, Thomas G. Hofmann, Peter J. McKinnon and Pierre-Olivier Frappart. Administrative, technical, or material support: David E. Reuss, Thomas G. Hofmann, Peter J. McKinnon, Andreas von Deimling and Pierre-Olivier Frappart. Study supervision: David E. Reuss and Pierre-Olivier Frappart.

ACKNOWLEDGEMENTS

CONFLICTS OF INTEREST STATEMENT

No potential conflicts of interest were disclosed by the other authors.

DATA AVAILABILITY STATEMENT

The data that support the findings of this study are available from the corresponding author upon reasonable request.

ETHICS STATEMENT

All animal care and procedures followed German legal regulations and were previously approved by the governmental review board of the state of Baden-Württemberg (Regierungspräsidium Karlsruhe-Abteilung 3-Landwirtschaft, Ländlicher Raum, Veterinär-und Lebensmittelwesen). All aspects of the mouse work were carried out following strict guidelines to ensure careful, consistent and ethical handling of mice. Human tumour tissues were obtained from the archives of the Department of Neuropathology and the Department of Neurosurgery at the Heidelberg University Hospital. Research use of tissues and anonymisation of data were in accordance with local ethical approvals.

ORCID

Felix Sahm https://orcid.org/0000-0001-5441-1962

REFERENCES

1. Lengauer C, Kinzler KW, Vogelstein B. Genetic instabilities in human cancers. *Nature*. 1998;396(6712):643-649. doi:10.1038/25292
2. Frappart PO, McKinnon PJ. Ataxia-telangiectasia and related diseases. *Neuromolecular Med*. 2006;8(4):495-511. doi:10.1385/NMM:8:4:495
3. Chrzanowska KH, Gregorek H, Dembowska-Baginska B, Kalina MA, Digweed M. Nijmegen breakage syndrome (NBS). *Orphanet J Rare Dis*. 2012;7(1):13. doi:10.1186/1750-1172-7-13
4. Meyer S, Kingston H, Taylor AM, et al. Rhabdomyosarcoma in Nijmegen breakage syndrome: strong association with perianal primary site. *Cancer Genet Cytogenet*. 2004;154(2):169-174. doi:10.1016/j.cancergencyto.2004.02.022
5. Tekin M, Dogu F, Tacyildiz N, et al. 657del5 mutation in the NBS1 gene is associated with Nijmegen breakage syndrome in a Turkish family. *Clin Genet*. 2002;62(1):84-88. doi:10.1034/j.1399-0004.2002.620112.x
6. Der Kaloustian VM, Kleijer W, Booth A, et al. Possible new variant of Nijmegen breakage syndrome. *Am J Med Genet*. 1996;65(1):21-26. doi:10.1002/(SICI)1096-8628(19961002)65:13.0.CO;2-0
7. Distel L, Neubauer S, Varon R, Holter W, Grabenbauer G. Fatal toxicity following radio- and chemotherapy of medulloblastoma in a child with unrecognized Nijmegen breakage syndrome. *Med Pediatr Oncol*. 2003;41(1):44-48. doi:10.1002/mpo.10275
8. Cybulski C, Wokolorczyk D, Kluzniak W, et al. An inherited NBN mutation is associated with poor prognosis prostate cancer. *Br J Cancer*. 2013;108(2):461-468. doi:10.1038/bjc.2012.486
9. Cybulski C, Gorski B, Debniak T, et al. NBS1 is a prostate cancer susceptibility gene. *Cancer Res*. 2004;64(4):1215-1219. doi:10.1158/0008-5472.CAN-03-2502
10. Plisiecka-Halasa J, Dansonka-Mieszkowska A, Rembiszewska A, Bidzinski M, Steffen J, Kupryjanczyk J. Nijmegen breakage syndrome gene (NBS1) alterations and its protein (nibrin) expression in human ovarian tumours. *Ann Hum Genet*. 2002;66(6):353-359. doi:10.1046/j.1469-1809.2002.00122.x
11. Steffen J, Maneva G, Poplawska L, Varon R, Mioduszewska O, Sperling K. Increased risk of gastrointestinal lymphoma in carriers of the 657del5 NBS1 gene mutation. *Int J Cancer*. 2006;119(12):2970-2973. doi:10.1002/ijc.22280
12. Steffen J, Varon R, Mosor M, et al. Increased cancer risk of heterozygotes with NBS1 germline mutations in Poland. *Int J Cancer*. 2004;111(1):67-71. doi:10.1002/ijc.20239
13. Bogdanova N, Feshchenko S, Schurmann P, et al. Nijmegen breakage syndrome mutations and risk of breast cancer. *Int J Cancer*. 2008;122(4):802-806. doi:10.1002/ijc.23168
14. Bogdanova N, Schurmann P, Waltes R, et al. NBS1 variant I171V and breast cancer risk. *Breast Cancer Res Treat*. 2008;112(1):75-79. doi:10.1007/s10549-007-9820-4
15. Gorski B, Debniak T, Masojc B, et al. Germline 657del5 mutation in the NBS1 gene in breast cancer patients. *Int J Cancer*. 2003;106(3):379-381. doi:10.1002/ijc.11231
16. Nowak J, Mosor M, Ziolkowska I, et al. Heterozygous carriers of the I171V mutation of the NBS1 gene have a significantly increased risk of solid malignant tumours. *Eur J Cancer*. 2008;44(4):627-630. doi:10.1016/j.ejca.2008.01.006
17. Debniak T, Gorski B, Cybulski C, et al. Germline 657del5 mutation in the NBS1 gene in patients with malignant melanoma of the skin. *Melanoma Res*. 2003;13(4):365-370. doi:10.1097/00008390-200308000-00005
18. Lener MR, Scott RJ, Kluzniak W, et al. Do founder mutations characteristic of some cancer sites also predispose to pancreatic cancer? *Int J Cancer*. 2016;139(3):601-606. doi:10.1002/ijc.30116
19. Borecka M, Zemankova P, Lhota F, et al. The c.657del5 variant in the NBN gene predisposes to pancreatic cancer. *Gene*. 2016;587(2):169-172. doi:10.1016/j.gene.2016.04.056

20. Mosor M, Ziolkowska I, Januszkiewicz-Lewandowska D, Nowak J. Polymorphisms and haplotypes of the NBS1 gene in childhood acute leukaemia. *Eur J Cancer*. 2008;44(15):2226-2232. doi:10.1016/j.ejca.2008.06.026

21. Zhu J, Petersen S, Tessarollo L, Nussenzweig A. Targeted disruption of the Nijmegen breakage syndrome gene NBS1 leads to early embryonic lethality in mice. *Curr Biol*. 2001;11(2):105-109. doi:10.1016/S0960-9822(01)00019-7

22. Dumon-Jones V, Frappart PO, Tong WM, et al. Nbn heterozygosity renders mice susceptible to tumor formation and ionizing radiation-induced tumorigenesis. *Cancer Res*. 2003;63(21):7263-7269.

23. Kang J, Bronson RT, Xu Y. Targeted disruption of NBS1 reveals its roles in mouse development and DNA repair. *EMBO j*. 2002;21(6):1447-1455. doi:10.1093/emboj/21.6.1447

24. Frappart PO, Tong WM, Demuth I, et al. An essential function for NBS1 in the prevention of ataxia and cerebellar defects. *Nat Med*. 2005;11(5):538-544. doi:10.1038/nm1228

25. Frappart PO, Lee Y, Russell HR, et al. Recurrent genomic alterations characterize medulloblastoma arising from DNA double-strand break repair deficiency. *Proc Natl Acad Sci U S a*. 2009;106(6):1880-1885. doi:10.1073/pnas.0806882106

26. Yan CT, Kaushal D, Murphy M, et al. XRCC4 suppresses medulloblastomas with recurrent translocations in p53-deficient mice. *Proc Natl Acad Sci U S a*. 2006;103(19):7378-7383. doi:10.1073/pnas.0601938103

27. Frappart PO, Lee Y, Lamont J, McKinnon PJ. BRCA2 is required for neurogenesis and suppression of medulloblastoma. *EMBO j*. 2007;26(11):2732-2742. doi:10.1038/sj.emboj.7601703

28. Rodrigues PM, Grigaravicius P, Remus M, et al. Nbn and atm cooperate in a tissue and developmental stage-specific manner to prevent double strand breaks and apoptosis in developing brain and eye. *PLoS ONE*. 2013;8(7):e69209. doi:10.1371/journal.pone.0069209

29. Dobin A, Davis CA, Schlesinger F, et al. STAR: ultrafast universal RNA-seq aligner. *Bioinformatics*. 2013;29(1):15-21. doi:10.1093/bioinformatics/bts635

30. Reuss DE, Piro RM, Jones DT, et al. Secretory meningiomas are defined by combined KLF4 K409Q and TRAF7 mutations. *Acta Neuropathol*. 2013;125(3):351-358. doi:10.1007/s00401-013-1093-x

31. Sahm F, Schrimpf D, Jones DT, et al. Next-generation sequencing in routine brain tumor diagnostics enables an integrated diagnosis and identifies actionable targets. *Acta Neuropathol*. 2016;131(6):903-910. doi:10.1007/s00401-015-1519-8

32. Stichel D, Schrimpf D, Casalini B, et al. Routine RNA sequencing of formalin-fixed paraffin-embedded specimens in neuropathology diagnostics identifies diagnostically and therapeutically relevant gene fusions. *Acta Neuropathol*. 2019;138(5):827-835. doi:10.1007/s00401-019-02039-3

33. Mootha VK, Lindgren CM, Eriksson KF, et al. PGC-1alpha-responsive genes involved in oxidative phosphorylation are coordinately down-regulated in human diabetes. *Nat Genet*. 2003;34(3):267-273. doi:10.1038/ng1180

34. Subramanian A, Tamayo P, Mootha VK, et al. Gene set enrichment analysis: a knowledge-based approach for interpreting genome-wide expression profiles. *Proc Natl Acad Sci U S a*. 2005;102(43):15545-15550. doi:10.1073/pnas.0506580102

35. Verhaak RG, Hoadley KA, Purdom E, et al. Integrated genomic analysis identifies clinically relevant subtypes of glioblastoma characterized by abnormalities in PDGFRA, IDH1, EGFR, and NF1. *Cancer Cell*. 2010;17(1):98-110. doi:10.1016/j.ccr.2009.12.020

36. Cahoy JD, Emery B, Kaushal A, et al. A transcriptome database for astrocytes, neurons, and oligodendrocytes: a new resource for understanding brain development and function. *J Neurosci*. 2008;28(1):264-278. doi:10.1523/JNEUROSCI.4178-07.2008

37. Brennan CW, Verhaak RG, McKenna A, et al. The somatic genomic landscape of glioblastoma. *Cell*. 2013;155(2):462-477. doi:10.1016/j.cell.2013.09.034

38. Cancer Genome Atlas Research N. Comprehensive genomic characterization defines human glioblastoma genes and core pathways. *Nature*. 2008;455(7216):1061-1068. doi:10.1038/nature07385

39. Jones DT, Jager N, Kool M, et al. Dissecting the genomic complexity underlying medulloblastoma. *Nature*. 2012;488(7409):100-105. doi:10.1038/nature11284

40. Morrissy AS, Garzia L, Shih DJ, et al. Divergent clonal selection dominates medulloblastoma at recurrence. *Nature*. 2016;529(7586):351-357. doi:10.1038/nature16478

41. Northcott PA, Buchhalter I, Morrissy AS, et al. The whole-genome landscape of medulloblastoma subtypes. *Nature*. 2017;547(7663):311-317. doi:10.1038/nature22973

42. Pugh TJ, Weeraratne SD, Archer TC, et al. Medulloblastoma exome sequencing uncovers subtype-specific somatic mutations. *Nature*. 2012;488(7409):106-110. doi:10.1038/nature11329

43. Robinson G, Parker M, Kranenburg TA, et al. Novel mutations target distinct subgroups of medulloblastoma. *Nature*. 2012;488(7409):43-48. doi:10.1038/nature11213

44. Vaubel RA, Tian S, Remonde D, et al. Genomic and phenotypic characterization of a broad panel of patient-derived xenografts reflects the diversity of glioblastoma. *Clin Cancer Res*. 2020;26(5):1094-1104. doi:10.1158/1078-0432.CCR-19-0909

45. Wang LB, Karpova A, Gritsenko MA, et al. Proteogenomic and metabolomic characterization of human glioblastoma. *Cancer Cell*. 2021;39(509–528):e520.

46. Zhao J, Chen AX, Gartrell RD, et al. Immune and genomic correlates of response to anti-PD-1 immunotherapy in glioblastoma. *Nat Med*. 2019;25(3):462-469. doi:10.1038/s41591-019-0349-y

47. Seidel P, Remus M, Delacher M, et al. Epidermal Nbn deletion causes premature hair loss and a phenotype resembling psoriasiform dermatitis. *Oncotarget*. 2016;7(17):23006-23018. doi:10.18632/oncotarget.8470

48. Huang MD, Chen XF, Xu G, et al. Genetic variation in the NBS1 gene is associated with hepatic cancer risk in a Chinese population. *DNA Cell Biol*. 2012;31(5):678-682. doi:10.1089/dna.2011.1421

49. Watanabe T, Nobusawa S, Lu S, Huang J, Mittelbronn M, Ohgaki H. Mutational inactivation of the Nijmegen breakage syndrome gene (NBS1) in glioblastomas is associated with multiple TP53 mutations. *J Neuropathol Exp Neurol*. 2009;68(2):210-215. doi:10.1097/NEN.0b013e31819724c2

50. Galvao RP, Kasina A, McNeill RS, et al. Transformation of quiescent adult oligodendrocyte precursor cells into malignant glioma through a multistep reactivation process. *Proc Natl Acad Sci U S a*. 2014;111(40):E4214-E4223. doi:10.1073/pnas.1414389111

51. Li R, Yang YG, Gao Y, Wang ZQ, Tong WM. A distinct response to endogenous DNA damage in the development of Nbs1-deficient cortical neurons. *Cell Res*. 2012;22(5):859-872. doi:10.1038/cr.2012.3

52. Campisi J. Aging, cellular senescence, and cancer. *Annu Rev Physiol*. 2013;75(1):685-705. doi:10.1146/annurev-physiol-030212-183653

53. Petroni M, Fabretti F, Giulio SD, et al. A gene dosage-dependent effect unveils NBS1 as both a haploinsufficient tumour suppressor and an essential gene for SHH-medulloblastoma. *Neuropathol Appl Neurobiol*. 2022;48(6):e12837. doi:10.1111/nan.12837

54. Ciara E, Piekutowska-Abramczuk D, Popowska E, et al. Heterozygous germ-line mutations in the NBN gene predispose to medulloblastoma in pediatric patients. *Acta Neuropathol*. 2010;119(3):325-334. doi:10.1007/s00401-009-0608-y

55. Kondratenko I, Paschenko O, Polyakov A, Bologov A. Nijmegen breakage syndrome. *Adv Exp Med Biol*. 2007;601:61-67. doi:10.1007/978-0-387-72005-0_6

56. Bakhshi S, Cerosaletti KM, Concannon P, et al. Medulloblastoma with adverse reaction to radiation therapy in Nijmegen breakage

syndrome. *J Pediatr Hematol Oncol*. 2003;25(3):248-251. doi:10.1097/00043426-200303000-00013

57. Williams BR, Mirzoeva OK, Morgan WF, Lin J, Dunnick W, Petrini JH. A murine model of Nijmegen breakage syndrome. *Curr Biol*. 2002;12(8):648-653. doi:10.1016/S0960-9822(02)00763-7

58. Difilippantonio S, Celeste A, Fernandez-Capetillo O, et al. Role of Nbs1 in the activation of the Atm kinase revealed in humanized mouse models. *Nat Cell Biol*. 2005;7(7):675-685. doi:10.1038/ncb1270

59. Huse JT, Holland EC. Genetically engineered mouse models of brain cancer and the promise of preclinical testing. *Brain Pathol*. 2009;19(1):132-143. doi:10.1111/j.1750-3639.2008.00234.x

60. Chow LM, Endersby R, Zhu X, et al. Cooperativity within and among Pten, p53, and Rb pathways induces high-grade astrocytoma in adult brain. *Cancer Cell*. 2011;19(3):305-316. doi:10.1016/j.ccr.2011.01.039

61. Kroonen J, Nassen J, Boulanger YG, et al. Human glioblastoma-initiating cells invade specifically the subventricular zones and olfactory bulbs of mice after striatal injection. *Int J Cancer*. 2011;129(3):574-585. doi:10.1002/ijc.25709

62. Wu G, Diaz AK, Paugh BS, et al. The genomic landscape of diffuse intrinsic pontine glioma and pediatric non-brainstem high-grade glioma. *Nat Genet*. 2014;46(5):444-450. doi:10.1038/ng.2938

63. Rizzo D, Ruggiero A, Martini M, Rizzo V, Maurizi P, Riccardi R. Molecular biology in pediatric high-grade glioma: impact on prognosis and treatment. *Biomed Res Int*. 2015;2015:215135. doi:10.1155/2015/215135

64. Clarke M, Mackay A, Ismer B, et al. Infant high-grade gliomas comprise multiple subgroups characterized by novel targetable gene fusions and favorable outcomes. *Cancer Discov*. 2020;10(7):942-963. doi:10.1158/2159-8290.CD-19-1030

65. DeSisto J, Lucas JT Jr, Xu K, et al. Comprehensive molecular characterization of pediatric radiation-induced high-grade glioma. *Nat Commun*. 2021;12(1):5531. doi:10.1038/s41467-021-25709-x

66. Deng MY, Sturm D, Pfaff E, et al. Radiation-induced gliomas represent H3-/IDH-wild type pediatric gliomas with recurrent PDGFRA amplification and loss of CDKN2A/B. *Nat Commun*. 2021;12(1):5530. doi:10.1038/s41467-021-25708-y

67. Lopez GY, Van Ziffle J, Onodera C, et al. The genetic landscape of gliomas arising after therapeutic radiation. *Acta Neuropathol*. 2019;137(1):139-150. doi:10.1007/s00401-018-1906-z

68. Yamanaka R, Hayano A, Kanayama T. Radiation-induced gliomas: a comprehensive review and meta-analysis. *Neurosurg Rev*. 2018;41(3):719-731. doi:10.1007/s10143-016-0786-8

69. Camacho CV, Todorova PK, Hardebeck MC, et al. DNA double-strand breaks cooperate with loss of Ink4 and Arf tumor suppressors to generate glioblastomas with frequent met amplification. *Oncogene*. 2015;34(8):1064-1072. doi:10.1038/onc.2014.29

70. Todorova PK, Fletcher-Sananikone E, Mukherjee B, et al. Radiation-induced DNA damage cooperates with heterozygosity of TP53 and PTEN to generate high-grade gliomas. *Cancer Res*. 2019;79(14):3749-3761. doi:10.1158/0008-5472.CAN-19-0680

71. Hellman A, Zlotorynski E, Scherer SW, et al. A role for common fragile site induction in amplification of human oncogenes. *Cancer Cell*. 2002;1(1):89-97. doi:10.1016/S1535-6108(02)00017-X

72. Glover TW, Wilson TE, Arlt MF. Fragile sites in cancer: more than meets the eye. *Nat Rev Cancer*. 2017;17(8):489-501. doi:10.1038/nrc.2017.52

73. Wang H, Li Y, Truong LN, et al. CtIP maintains stability at common fragile sites and inverted repeats by end resection-independent endonuclease activity. *Mol Cell*. 2014;54(6):1012-1021. doi:10.1016/j.molcel.2014.04.012

74. Chang EY, Tsai S, Aristizabal MJ, et al. MRE11-RAD50-NBS1 promotes Fanconi anemia R-loop suppression at transcription-replication conflicts. *Nat Commun*. 2019;10(1):4265. doi:10.1038/s41467-019-12271-w

75. Wardlaw CP, Petrini JHJ. ISG15 conjugation to proteins on nascent DNA mitigates DNA replication stress. *Nat Commun*. 2022;13(1):5971. doi:10.1038/s41467-022-33535-y

76. Takeda S, Hoa NN, Sasanuma H. The role of the Mre11-Rad50-Nbs1 complex in double-strand break repair-facts and myths. *J Radiat Res*. 2016;57(Suppl 1):i25-i32. doi:10.1093/jrr/rrw034

SUPPORTING INFORMATION

Additional supporting information can be found online in the Supporting Information section at the end of this article.